Development of carbon adsorbents with high surface acidic and basic group contents from phosphoric acid activation of xylitol

Article *in* RSC Advances · September 2015

DOI: 10.1039/C5RA14579A

CITATIONS
16

READS
661

7 authors, including:

Hai Liu
Shandong University
44 PUBLICATIONS **2,567** CITATIONS
SEE PROFILE

Jian Zhang
International Peace Maternity and Child Health Hospital
1,108 PUBLICATIONS **49,272** CITATIONS
SEE PROFILE

Yan Kang
Qingdao University of Science and Technology
311 PUBLICATIONS **4,334** CITATIONS
SEE PROFILE

Cheng Cheng
Chongqing University
33 PUBLICATIONS **907** CITATIONS
SEE PROFILE

RSC Advances

PAPER

View Article Online
View Journal | View Issue

Cite this: *RSC Adv.*, 2015, **5**, 81220

Development of carbon adsorbents with high surface acidic and basic group contents from phosphoric acid activation of xylitol†

Hai Liu,[ab] Jian Zhang,*[a] Li Jiang,[a] Yan Kang,[a] Cheng Cheng,[a] Zizhang Guo[a] and Chenglu Zhang[a]

Received 23rd July 2015
Accepted 16th September 2015

DOI: 10.1039/c5ra14579a

www.rsc.org/advances

The present paper evaluated the feasibility of synthetizing activated carbons from xylitol with phosphoric acid activation at mild temperatures. Activation temperature (250–450 °C) and phosphoric acid to xylitol impregnation ratio (0.2–3 wt%) were varied during the synthesis of xylitol-based activated carbon, and the effects of these parameters on the textural and chemical properties of the final activated carbons were investigated by XRD, Raman, N_2 adsorption and desorption, SEM, XPS and Boehm's titration. The results of yield, XRD and Raman indicated that phosphoric acid activation enhanced the yields of activated carbons, and facilitated the formation of completely carbonized materials at low temperatures (around 250 °C) by comparing with charcoals derived from pyrolysis of xylitol. The porous structures of the activated carbons were developed after activation, and for each activation temperature, the carbons reached the maximum surface area at an impregnation ratio of 1.5. Due to the strong oxidizing radicals decomposed from phosphates, the produced carbons contain relatively high concentrations of acidic and basic surface groups. The total surface groups peaked at 6.08 mmol g^{-1} for activated carbon obtained at an activation temperature of 350 °C and impregnation ratio of 1.5. The Ni(II) adsorption capacity of the activated carbons was 4 to 7 folds that of the charcoals.

1. Introduction

Activated carbon has been well proven to be one of the most effective adsorbents toward a wide variety of organic and inorganic pollutants from aqueous or gaseous environments due to its highly developed porous structure, low acid/base reactivity, and wide spectrum of surface functional groups.[1–3] In general, activated carbon production consists of two processes: chemical activation and physical activation. Due to the low reactivity between physical activating agents (H_2O or CO_2) and carbon precursors, high activation temperatures (>800 °C) and prolonged times are required.[4–6] Their high surface area comes at the cost of a high extent of char burn-off, resulting in low product yield and scarce surface functional groups. The chemical activation usually takes place at lower temperatures (about 400–700 °C) in the presence of an activating agent ($ZnCl_2$ or H_3PO_4). Therefore, the produced activated carbons contain well-developed structure, high yield and favorable surface chemistry. Given the environmental and economic effects, phosphoric acid activation has been well demonstrated to be a promising method.[7,8]

A various carbonaceous materials have been used as precursors to prepare activated carbons by phosphoric acid activation, such as lignocellulosic materials,[9,10] synthetic polymers,[11,12] and coals.[13,14] Impregnation and activation are the main processes involved in phosphoric acid activation. During impregnation stage, H_3PO_4 permeates into the carbonaceous material and forms macromolecule composites. For subsequent activation, H_3PO_4 reacts with precursor, resulting in favorable physicochemical properties. Thus, the degree of impregnation affects dramatically the activation effects.[15,16] Since these precursors are polymeric or extremely stable, phosphoric acid is hard to react with them and penetrate into them at moderate conditions. Zuo *et al.* has reported that the impregnation time of 10 h could result in an 80% increase in surface area.[17] Therefore, in order to ensure good impregnation effects, the impregnation is required 6–24 h. It has been also reported the activation temperature should be controlled above 400 °C to ensure the produced activated carbons with well-developed structure or good surface chemical properties.[18–20] As a result,

[a]*Shandong Key Laboratory of Water Pollution Control and Resource Reuse, School of Environmental Science and Engineering, Shandong University, Jinan 250100, China. E-mail: zhangjian00@sdu.edu.cn; shandaliuhai@berkeley.edu; Fax: +86 531 88364513; Tel: +86 531 88363015*

[b]*Department of Chemical and Biomolecular Engineering, University of California, Berkeley, California 94720, USA*

† Electronic supplementary information (ESI) available: Table S1 summarizes the Langmuir model fitting parameters of the nickel adsorption onto the carbons. Fig. S1 presents Raman spectra and intensity ratios of D to G bands of the activated carbons. Fig. S2 presents SEM micrographs of C-*X* and AC samples. See DOI: 10.1039/c5ra14579a

producing activated carbon with phosphoric acid activation is a time and energy-consuming process.

As the most important heterogeneous element, oxygen can form different complexes with carbon, and result in acid–base and electron-donor/-acceptor properties of activated carbon. Surface functional groups of activated carbon give significant contribution to its adsorption ability, especially for low-size and positively charged heavy metal ions,[21,22] primarily through providing adsorption sites of proton exchange, electrostatic attraction, and surface complexation. Typical phosphoric acid activated carbons exhibit a wide distribution of pore size, but relatively low metal ions adsorption. Considering the huge influence of surface chemistry on the adsorption performance of carbon materials, various modification methods have been developed to increase surface oxygen content through pre- and post-treatment with gaseous or liquid chemicals.[23–25] However, these methods require an additional process and are also time and energy consuming process.

Organophosphorus compounds, as a kind of ester of phosphoric acid and alcohol, have been well demonstrated to be novel activating agents for developing activated carbons from lignocellulosic materials with relatively high surface oxygenated groups and heavy metal ions adsorption capacities in comparison with reference activated derived from H_3PO_4 activation in our previous works.[26–28] These favorable results were mainly contributed to that radicals ($R^{\bullet}$ and $RO^{\bullet}$) decomposed from phosphates further created the porosity and surface functional groups of final carbons. In general, the different properties of phosphoric acid-activated carbon mainly depend on the precursor nature and synthesis conditions. Polyhydric alcohols contain multiple hydroxyl groups, and they can condense with phosphoric acid *via* esterification to form low molecular weight phosphates. These compounds can be easily decomposed into phosphorus oxides and radicals. Based on these results, we deduce that these reactions may promote the carbonization of polyhydric alcohols at low temperature, and enhance the surface oxygen contents of the produced carbon materials, eventually increasing their adsorption abilities toward heavy metal ions. In addition, polyhydric alcohols can be melted at low temperatures (above 93 to 95 °C) and dissolves easily in phosphoric acid solution (*e.g.* 85 wt%).[29] Thus, *via* phosphoric acid activation, using polyhydric alcohols as carbon precursors may avoid the problem of long impregnation time and high activation temperature for production of activated carbon from conventional lignocellulosic materials. However, little information is available on preparation of activated carbon from phosphoric acid activation of polyhydric alcohols.

Accordingly, a common polyhydric alcohol, xylitol, was chosen as carbon precursor. Xylitol (formula, $CH_2OH(CHOH)_3$-CH_2OH) is categorized as a polyalcohol or sugar alcohol. The main goals of the present work are to evaluate the feasibility of preparation of activated carbon from xylitol with phosphoric acid activation, and to provide a full understanding of the chemical properties and structural characteristics of the carbons. For these purposes, the thermal behaviors of xylitol treated with different impregnation ratios of phosphoric acid were studied. The effects of impregnation ratio and activation temperature on the development of pore structure and chemical characteristics were also investigated. The synthesized carbon materials were characterized by X-ray diffraction (XRD), N_2 adsorption and desorption, scanning electron microscopy (SEM), X-ray photoelectron spectroscopy (XPS), and analysis of Boehm's titration.

2. Experimental (materials and methods)

2.1. Synthesis of carbon adsorbents

In a typical synthesis, activated carbons were prepared by phosphoric acid activation of xylitol. Five grams of xylitol was mixed fully with phosphoric acid solution (85 wt%) at a impregnation ratio of 0.2 : 1–3 : 1 (g H_3PO_4/g xylitol). The nomenclature for the impregnated samples (xylitol-*R*) was the xylitol followed by a number indicating the impregnation ratio. After mixing, xylitol-*R* samples were immediately heated (heating rate of 10 °C min^{-1}) from room temperature to the desired temperature and maintained at this temperature for 1 hour under nitrogen atmosphere (100 mL min^{-1}) in a tube furnace. After cooling to room temperature, the samples were washed with deionized water until steady pH and absence of phosphate anions. Finally, the samples were dried at 105 °C for 9 h and grounded to obtain the particle size of 100/160 mesh (Model *Φ*200). The activated carbons obtained at activation temperature of *X* °C with impregnation ratio of *R* were referred to as AC-*X*-*R*. In order to evaluate the effect of phosphoric acid activation on the characteristics of final carbon materials, the charcoals (C-*X*) were also prepared by pyrolysis of xylitol at the same heating conditions.

2.2. Characterization

The thermal behaviors of the untreated xylitol and xylitol-*R* samples during carbonization/activation were evaluated with a thermal analyzer (TGA-50 analyzer). Samples were heated at a heating rate of 10 °C min^{-1} under nitrogen atmosphere (100 mL min^{-1}). The crystallinity of the produced AC-*X*-*R* samples was investigated by using a Rigaku D/MAX-YA diffractometer with Ni-filtered Cu Kα radiation as X-ray source. Raman spectra were collected with a Raman microscope (633 nm laser excitation, Renishaw inVia Raman microscope, UK). The textural properties were determined by N_2 adsorption/desorption at 77 K with a surface area analyzer (Quantachrome Corporation, USA). The structure and morphology were examined by a scanning electron microscopy (SEM) JSM-5610LV (10 kV, Jeol Company, Japan). The oxygenated acidic and basic surface groups were determined using the Boehm's titration method.[30] The surface elemental composition was studied by using an X-ray photoelectron spectrometer (XPS, Perkin-Elmer PHI 550 ESCA/SAM) with Mg Kα irradiation source. All the spectra were calibrated by setting C 1s to 284.6 eV. The adsorption abilities of the carbon adsorbents were evaluated by batch Ni(II) adsorption experiment.

3. Results and discussion

3.1. Thermal analysis

The thermogravimetric analysis (TGA) and derivative thermogravimetric (DTG) curves of the original and H_3PO_4-inpregnated xylitol samples are shown in Fig. 1. It can be seen from Fig. 1a that the weight loss for original xylitol began at temperature slightly higher than its boiling point of 216 °C, its weight loss rate slowed down as temperature above 350 °C (Fig. 1b), and a slight weight was observed when temperature was kept at 450 °C, indicating that the carbonization process was completed. However, the xylitol-*R* samples showed a major weight loss at temperature below 200 °C, which reflected that phosphoric acid promoted carbonization at low temperatures. From room temperature to about 100 °C, an initial weight loss was mainly due to the loss of moisture present in the xylitol-*R* samples. Some reactions were expected to be responsible for the dramatic weight loss for pyrolysis of xylitol-*R* samples at temperature blow 250 °C: (1) esterification between phosphoric acid and xylitol, which took place at temperatures above about 90 °C; (2) etherification between hydroxyl groups of xylitol catalyzed by phosphoric acid; and (3) condensation between phosphoric acid molecules (occurred at temperature above 213 °C). Meanwhile, the produced phosphates with low polymerization degree were instable at high temperature, and subsequently volatilized and decomposed into radicals and P_2O_5,[31,32] causing a further weight loss.

The thermal behaviors of xylitol-*R* samples were obviously different to other phosphoric acid–impregnated lignocellulose/coal samples.[31,33] During activation, xylitol formed easily phosphates with low polymerization degree, which tended to volatilize and decompose and led to less phosphoric compounds remaining in the samples. The loss of phosphorous species and production of radicals by decomposition of phosphates resulted in: (1) carbonization of xylitol at low temperature (see Fig. 2) (2) low yield (see Fig. 3); (4) suppressed formation of porous structure (see Fig. 4); (3) low surface phosphorus content (see Fig. 6); and (4) large surface oxygen content (see Fig. 6) for final carbon materials.

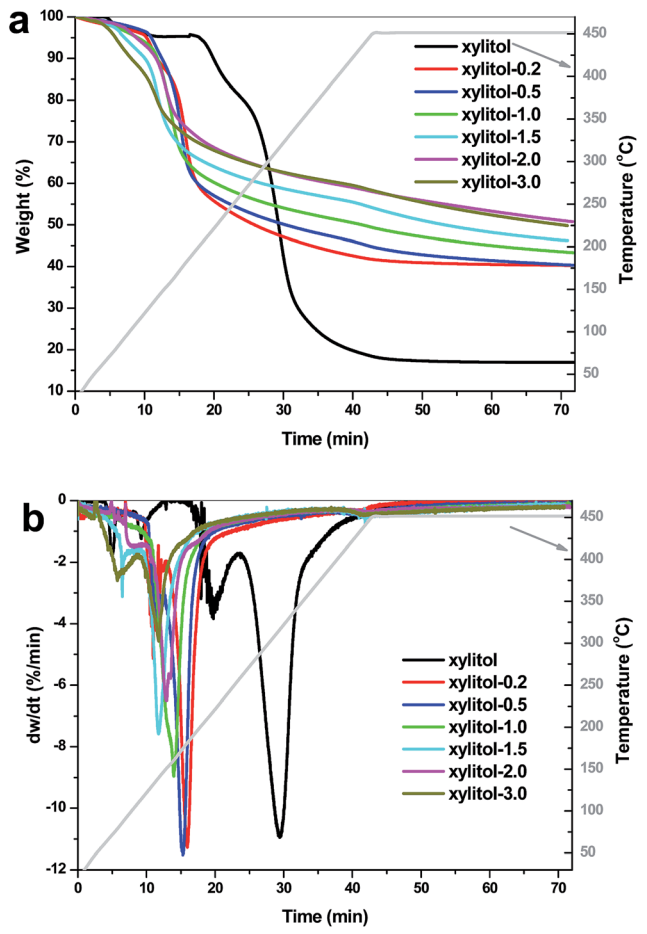

Fig. 1 TGA (a) and DTG (b) curves for pyrolysis of xylitol and xylitol-*R* samples.

3.2. Formation of carbon materials

As shown in Fig. 2, a broad peak at around $2\theta = 23°$ can be found from XRD patterns of some samples, which was attributed to (002) planes of the graphitic crystallites,[34] and revealing that these xylitol or xylitol-*R* samples have been carbonized or activated into carbon materials. All samples exhibited an intense and sharp peak at around $2\theta = 10°$, which was attributed to the water molecular or oxygen-containing groups between the layers of the graphite. It can be seen from Fig. 2a that for the C-*X* samples obtained at carbonization temperature below 350 °C, they exhibited a XRD pattern without (002) diffraction peak, reflecting that the final materials were carbonized incompletely. After phosphoric acid activation, absent, inconspicuous and broad (002) diffraction peaks were recognized for the AC-150-*R*, AC-200-*R* and AC-250-*R* samples (Fig. 2b–d), respectively. These results meant that phosphoric acid activation promoted the carbonization of xylitol at low temperatures, and the onset of complete carbonization of xylitol-*R* samples took place between 200 and 250 °C. The AC-250-*R* samples also exhibited typical Raman spectra of non-graphitic carbon materials (shown in (ESI) Fig. S1†). This can be also confirmed by the yield analysis that the yields of AC-200-*R* samples were slightly lower than that of AC-250-*R* samples (Fig. 3). Obviously, high activation temperature will promote the weight loss of xylitol-*R* samples (see Fig. 1). However, xylitol could not be incompletely carbonized at low activation temperature, hence some dissolved organic matters were removed from the solid products by DI water washing. Accordingly, it also can be deduced that AC-200-*R* samples were incomplete carbonized products. It is well known that xylitol has a very low melting point (93–95 °C) and can be dissolved in phosphoric acid solution easily. Thus, xylitol can be mixed fully with phosphoric acid, which promoted the reactions between xylitol and phosphoric acid. In addition, the formed phosphates decomposed into strong oxidizing radicals, and further enhanced the carbon structure forming at low temperature. Accordingly, the precursor exhibited high weight loss and formed carbonized structures at low temperatures.

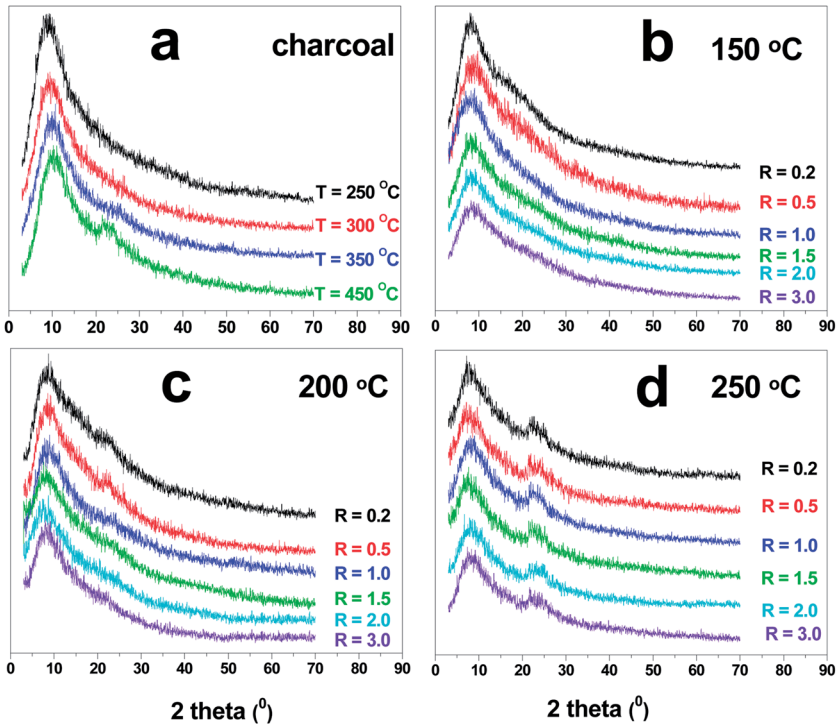

Fig. 2 XRD patterns of charcoals (a) derived from pyrolysis of xylitol and AC-*X*-*R* samples produced at activation temperatures of 150 (b), 200 (c), and 250 °C (d).

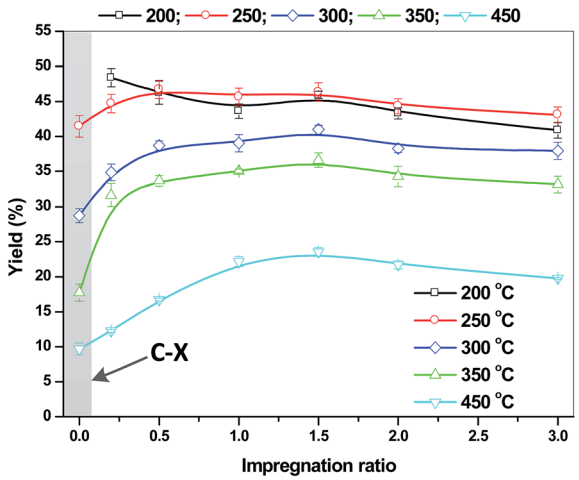

Fig. 3 Yields of the produced carbon materials (yield is defined as the % ratio of weight of carbon produced to the weight of xylitol utilized for activation/pyrolysis).

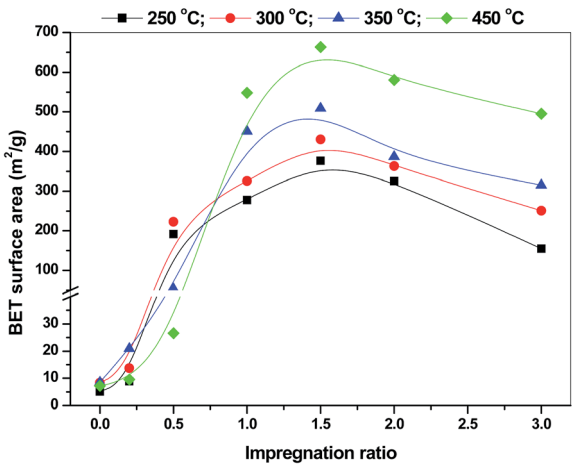

Fig. 4 BET surface area calculated by the standard BET method of the carbon materials.

The yields of the carbon materials are represented in Fig. 3. The yields of AC-*X*-*R* samples were obviously higher than that of C-*X* samples, especially at high activation or carbonization temperatures, meaning the good flame-retardant effect of phosphoric acid. This was due to that phosphoric acid promoted formation of carbon materials at low temperatures, hence increasing the yields of AC-*X*-*R* samples. For each activation temperature, with increasing impregnation ratio up to 3, the yield of the samples increased to a maximum at impregnation ratio of 1.5 and decreased slightly at higher impregnation ratios, because suitable dose of phosphoric acid had a positive effect on the yield, while the excessive dose resulted in the highly aggressive chemical reactions between the xylitol and phosphoric acid. For each impregnation ratio, the yield decreased dramatically as the reaction temperatures increased due to the enhanced decomposition of precursor at higher temperatures. It should be noted that AC-250-*R*, AC-300-*R* and AC-350-*R* samples had relatively high yields (30–45%) due to the low activation temperatures. However, the samples produced at activation temperature of 450 °C had low yields (10–20%). The yields of xylitol-based activated carbons were

much lower than the activated carbon derived from lignocellulose materials (30–50%) at activation temperature of 450 °C, such jackfruit peel waste,[18] kraft lignin,[35] date stones,[36] and rubber wood sawdust.[37] As proposed above, the oxidizing radicals derived from decomposition of phosphate esters accelerated the weight loss of xylitol-*R* samples, and the volatilization of organophosphorus esters also caused the relatively low yields of final carbon materials. Taking into account the yield and completely carbonized products, the activation temperature was recommended in the range of 250–450 °C for phosphoric acid xylitol-based carbon material production.

3.3. Physical properties of activated carbons

The effects of impregnation ratio and activation temperature on the BET surface area (S_{BET}) of the samples are shown in Fig. 4. At each activation temperature, the S_{BET} of carbons reached a maximum at an impregnation ratio of approximately 1.5, which was coincident with the results of yield. The same tendency was observed previously for activated carbons produced from phosphoric acid activation of cotton stalks,[32] hydrochars,[38] and cellulose.[39] It can be seen that phosphoric acid activation developed the porous structure of final carbon materials (AC-*X*-*R*) as compared to the C-*X* samples (less than 10 $m^2\ g^{-1}$), particularly for the AC-*X*-*R* samples with *R* beyond a value of 0.5. Such results can be also observed from the SEM images for the C-*X* and AC samples (shown in ESI Fig. S2†). With impregnation ratio below 0.5, the carbonization/activation was incomplete/inadequate for original xylitol and xylitol-*X*-0.2 samples, demonstrated by their low surface area (less than 30 $m^2\ g^{-1}$). Some phosphoric acid or phosphorous species in xylitol-*R* was lost *via* decomposition and volatilization of phosphates. Thus, detectable activation in the terms of porous structure was not obtained for xylotil-*X*-0.2 samples. Such phenomenon can be also observed from the S_{BET} of AC-*X*-0.5 samples that the S_{BET} values of AC-250-0.5 and AC-300-0.5 samples were much larger than AC-350-0.5 and AC-450-0.5 due to the loss of phosphoric acid and the consequent damage of pore structure at high activation temperatures. An increase in impregnation ratio enhanced degree of polymerization of phosphates, and restrained their thermal decomposition, resulting in the higher yield and surface area. However, the excessive phosphoric acid addition aggravated such activation effect and destroyed some pores.[32] The surface area of carbons increased with increasing activation temperature was mainly due to the enhanced interactions of phosphoric and xylitol. This trend was generally consistent with previous reports for phosphoric acid activation of kraft lignin,[35] chestnut wood,[40] and rice straw.[41,42]

Nitrogen adsorption and desorption isotherms and DFT pore size distributions of the carbons produced at different activation temperatures using an impregnation ratio of 1.5 are summarized in Fig. 5. The isotherms for AC-250-1.5 and AC-300-1.5 were Type I, practically without hysteresis loop, which was characteristic of highly microporous carbons. The isotherms for AC-350-1.5 and AC-450-1.5 were the mixture of Type I and IV, with a hysteresis at P/P_0 above 0.4 (Fig. 5a), indicating a micro-mesoporous structure. These results also can be confirmed

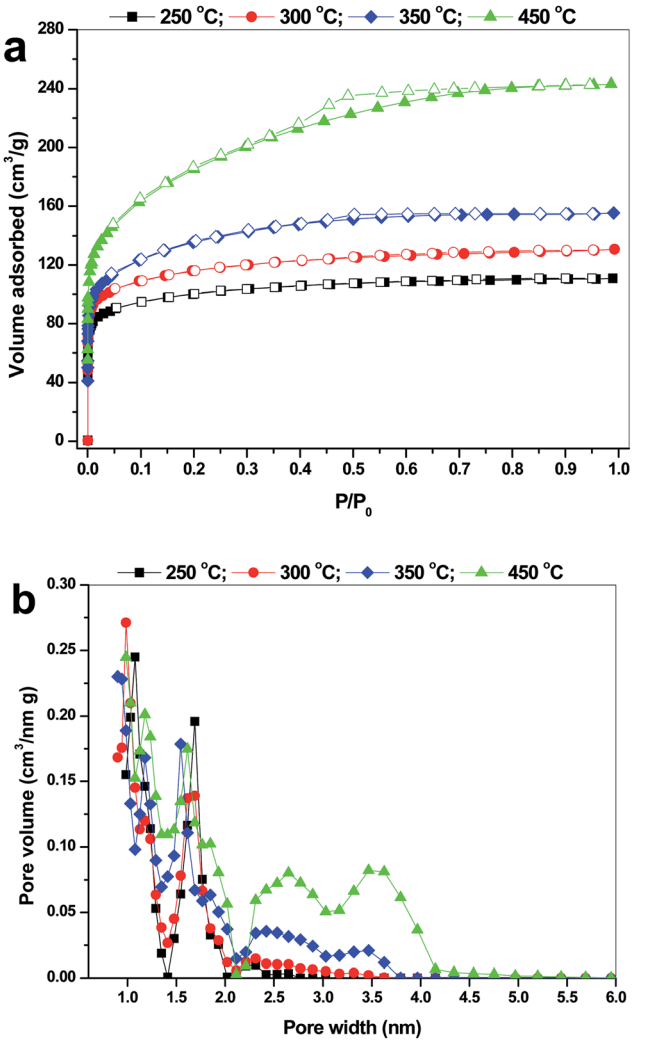

Fig. 5 N_2 adsorption/desorption isotherms (a) and DFT pore size distributions (b) for carbons prepared with impregnation ratio of 1.5 at different activation temperatures.

from Fig. 5b that the pore widths of a large part of pores for AC-350-1.5 and AC-450-1.5 were in the range of 2–6 nm, as will be demonstrated by the evaluated parameters (see Table 1). The structural characterization results listed in Table 1 showed that with the increase of temperature from 250 to 450 °C, the micropores and mesopores of the carbons were developed, but the contribution of micropore to the total porosity (V_{mic}/V_{mes}) decreased, suggesting the enlargement of existing micropores as well as the continuous pore creation.

The simultaneous increases of micropore and mesopore volumes were related to the geometry of polymeric species (polyphosphoric acids) and the production of volatile substances. By condensation and dehydration, phosphoric acid (H_3PO_4) converted to polycondensed forms: pyrophosphoric acid ($H_4P_2O_7$) and polyphosphoric acid ($H_{n+2}P_nO_{3n+1}$) at temperature above 213 °C, and metaphosphoric acid ($(HPO_3)_n$) (>300 °C).[31] After thermal treatment, the acids occupied different volumes in the carbonized materials were extracted by washing, and produced different porosities. The higher

Table 1 Textural parameters of activated carbons prepared with impregnation ratio of 1.5 at different activation temperatures[a]

Carbon	S_{BET} ($m^2\ g^{-1}$)	S_{mic} ($m^2\ g^{-1}$)	%	S_{ext} ($m^2\ g^{-1}$)	%	V_{tot} ($cm^3\ g^{-1}$)	V_{mic} ($m^3\ g^{-1}$)	%	V_{ext} ($m^3\ g^{-1}$)	%
AC-250-1.5	377	372	98.7	5	1.3	0.171	0.165	96.5	0.006	3.5
AC-300-1.5	432	380	88.0	52	12.0	0.202	0.169	83.7	0.033	16.3
AC-350-1.5	509	403	79.2	106	20.8	0.248	0.173	69.8	0.075	30.2
AC-450-1.5	663	433	65.3	230	34.7	0.376	0.178	47.3	0.198	52.7

[a] The micropore surface area (S_{mic}), external surface area (S_{ext}) and micropore volume (V_{mic}) were evaluated by the *t*-plot method. Total pore volume calculated for $P/P_0 = 0.95$. Mesopore volume (V_{mes}) was calculated by $V_{tot} - V_{mic}$.

activation temperature promoted the condensation and dehydration of phosphoric acid, hence causing the formation of larger pores. Thus, evident pore evolution occurred as activation temperature was above 300 °C. Meanwhile, phosphoric acid formed cross-linked structure with polyhydric alcohol (xylitol), and the enhanced elimination of highly volatile matters at higher activation temperatures further promoted the porosity of final carbons.

3.4. Chemical characteristics

The surface compositions of the carbons were also determined by XPS shown in Fig. 6. The spectra indicated the presence of two distinct peaks for carbon and oxygen elements, and the contribution of other elements was insignificant, meaning the functionalities were derived from the complexes of carbon and/or oxygen. Obviously, in comparison with C-*X* samples, the much higher intensity of O 1s peaks for the activated carbons derived from same heating conditions indicated that they contained more oxygen containing groups. The XPS can only reflect the oxygen functionalities on the outer surface of the samples. The activated carbons exhibited porous structure and the C-*X* samples were almost nonporous. It meant the activated carbons exhibited extra more total oxygen groups than C-*X* samples. For the phosphoric acid activated carbons, high phosphorus content (1–8 wt%) were detected on their surfaces.[7,43,44] However, the activated carbon studied in present paper was absent of phosphorus species, which can be attributed the formation, and subsequent volatilization and decomposition of phosphate esters.

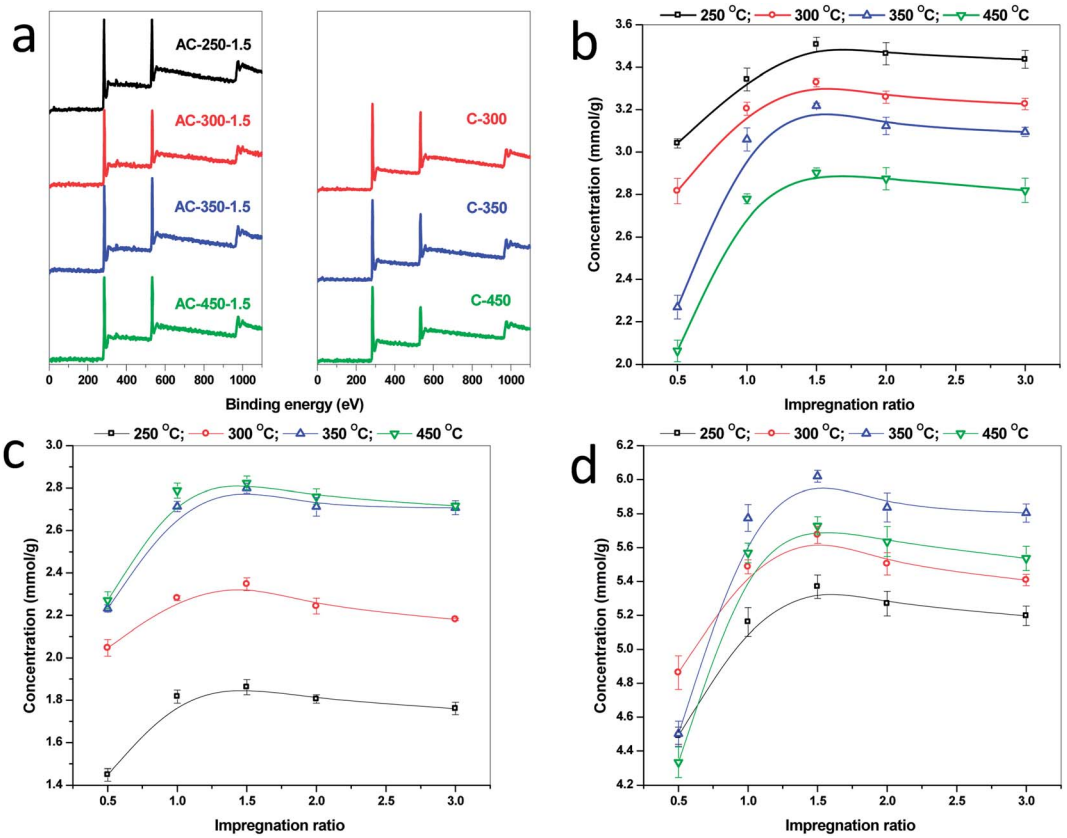

Fig. 6 XPS survey spectra of C-*X* and AC-*X*-1.5 samples (a). The Boehm's titration results of the carbons: acidity (b), basicity (c), and total groups (d).

In order to evaluate quantitatively the surface functionalities of the carbon influenced by the preparation parameters, both acidic and basic groups of the activated carbon were determined by Boehm' titration. It is known that the acidity of activated carbon mainly derive from the carboxylic acids, lactones and phenolic hydroxyls, and basic groups originate from the complex aromatic system (delocalized π electrons) of graphene surface. During activation, many strong oxidizing radicals were produced, and eventually caused the high oxygen content of the final carbon materials. For these samples, increasing activation temperature reduced the amount of acidic groups and promoted the production of basic groups (see Fig. 6a and b). The high temperature led to the decomposition of acidic groups into CO and CO_2, since they are unstable at high temperature.[39] Meanwhile, the high temperature promoted the formation of delocalized π electrons, resulting in the high basicity.[18] When impregnation ratio increased from 0.5 to 1.0, both acidic and basic groups increased dramatically and reached a maximum at impregnation ratio of 1.5, then with impregnation ratio greater than 1.5, the amounts of these groups exhibited a slight decrease and kept high levels. As well demonstrated above that the phosphates decomposed and volatilized easily at low temperatures, during activation, less phosphoric compounds were left in the xylitol-0.2 and xylitol-0.5 samples, thus the formed oxygen groups were susceptible to the high temperature and decomposed into carbon gases. The larger impregnation ratio promoted the formation of phosphates with high degree of polymerization that tended to be stable at high temperature, whereas the large amount of phosphoric acid could hinder the thermal degradation of the oxygen groups. Accordingly, the carbon samples exhibited a slightly decrease in acidic groups with increasing impregnation ratio.

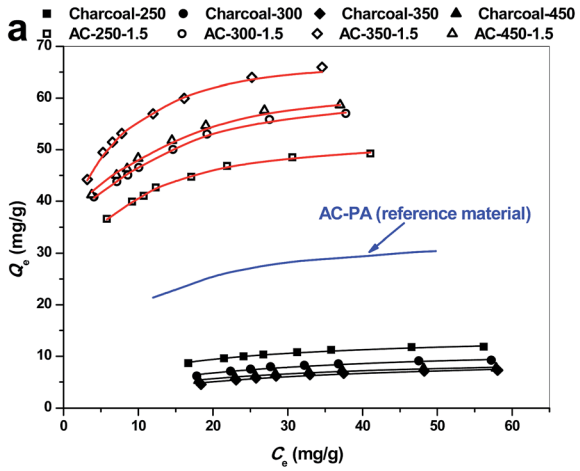

Fig. 7 Adsorption isotherms of Ni(II) for the carbons, fitted with Langmuir isotherm model (dosage = 0.2 g L^{-1}, initial Ni(II) concentrations = 20–60 mg L^{-1}, initial pH = 6.0 ± 0.02, temperature = 25 ± 2 °C, and ionic strength = 10 mM NaCl).

3.5. Evaluation of Ni(II) adsorption ability

As discussed above, phosphoric acid activation of xylitol could produce activated carbons with high surface acidity and basicity. This is very interesting considering that the produced activated carbons have application potentials in heavy metal ions removal from aqueous solution. Thus, in the present study, the adsorption properties of the xylitol-based activated carbons were evaluated by studying uptake of nickel ions from aqueous solutions. Adsorption isotherms were performed by a batch method, where 10 mg of carbon sample was added into a 150 mL conical flask with 50 mL solution of Ni(II) with an initial solution pH of 6.0. To estimate the maximum adsorption capacities of the produced activated carbons, the adsorption data were fitted with the Langmuir model ($Q_e = Q_m K_L C_e/(1 + K_L C_e)$), where Q_e and C_e are the Ni(II) equilibrium adsorption capacity (mg g^{-1}) and concentration in solution (mg L^{-1}), Q_m is the monolayer adsorption capacity of the adsorbent (mg g^{-1}), K_L is the Langmuir isotherm constant (L mg^{-1}).

The fitting Langmuir data for Ni(II) adsorption onto the activated carbons and a reference activated carbon (AC-PA) prepared from phosphoric acid activation of *Phragmites australis* (properties: S_{BET} = 1220 m^2 g^{-1}, V_{tot} = 1.098 cm^3 g^{-1}, V_{mic} = 0.235 cm^3 g^{-1}, acidic groups = 1.644 mmol g^{-1}, basic groups = 1.125 mmol g^{-1}) are shown in Fig. 7. The relatively high values of R^2 (>0.98, ESI Table S1†) and good representation of the data (Fig. 7) indicated that the Langmuir isotherm model was favorable to describe the adsorption of Ni(II) on the carbon

Table 2 Ni(II) adsorption capacity of activated carbons developed from various precursor with phosphoric acid activation

		Activation		Adsorption				
Precursor	Impregnation ratio	Temperature °C	Time	C_0 mg L^{-1}	pH	S_{BET} m^2 g^{-1}	Q_m mg g^{-1}	References
Xylitol	1.5	250	1 h	20–60	6.0	377	52.9	This work
Xylitol	1.5	300	1 h	20–60	6.0	432	62.9	This work
Xylitol	1.5	350	1 h	20–60	6.0	509	69.4	This work
Xylitol	1.5	350	1 h	20–60	6.0	663	64.5	This work
Phragmites australis	1.5	450	1 h	20–60	6.0	1220	35.2	This work
Lotus stalk	2	450	1 h	—	—	1220	31.0	45
Prosopis ruscifolia wood	2	450	0.5 h	—	—	1638	7.6	46
Arundo donax L.	2	500	0.5 h	5–100	5.8	1194	25.8	47
Date stone	1.75	450	2 h	10–100	—	826	24.4	48
Wool waste	1.5	550	40 min	10–60	—	472	54.0	49

adsorbents. The Q_m of the carbons followed an order of AC-350-1.5 > AC-450-1.5 > AC-300-1.5 > AC-250-1.5 > AC-PA ≫ C-250 > C-300 > C-350 > C-450. In comparison with charcoal samples, the 4–7 times higher Ni(II) adsorption capacities of activated carbons was clear evidence that phosphoric acid activation improved dramatically their Ni(II) adsorption capacities. Compared with the reference material (AC-PA), the 170–230% larger Ni(II) adsorption capacities indicated that AC-*X*-*R* could be promising adsorbents in Ni(II) ions pollution cleanup. For the sake of further comparison, Table 2 also shows the Ni(II) adsorption capacities of other activated carbons by phosphoric acid activation. The AC-*X*-1.5 samples in this study showed relatively good adsorption capacities compared to the adsorbents. The difference in Q_m of the adsorbents seems to depend primarily on the surface functions, as proposed by previous papers.[26,50,51] Since the ionic diameter of Ni(II) is very low (0.138 nm), the surfaces of adsorbents are easily accessible for Ni(II) ions, and the narrow micropore could not withdraw Ni(II) effectively. Strong chemical interactions existed between the functional groups of activated carbon and Ni(II) cations, such as electrostatic attraction between the deprotonated acidic oxygenized groups (carboxylic, lactonic and phenolic groups) and Ni^{2+} ions, ion exchange between acidic groups and Ni^{2+} ions, and complexation between oxygen complexes and Ni^{2+} ions. Meanwhile, the basic groups (the delocalized π electron systems of graphene layer) can form electron donor–acceptor complexes with Ni^{2+} ions *via* the Lewis-acid–base interaction.

4. Conclusion

The results of this study demonstrated that phosphoric acid activation of xylitol could produce promising carbon adsorbents with high contents of surface groups and large Ni(II) adsorption capacities. The complete carbonization for phosphoric acid-treated xylitol samples took place between 200 °C and 250 °C. For each activation temperature, the carbon samples reached the maximum surface area, and content of surface groups at impregnation ratio of 1.5. Compared with the charcoal obtained from pyrolysis of xylitol, the activated carbon showed much larger yields, surface area, surface groups content, and Ni(II) adsorption capacity.

Acknowledgements

This work was supported by the Independent Innovation Foundation of Shandong University (2012JC029), Natural Science Foundation for Distinguished Young Scholars of Shandong Province (JQ201216) and National Water Special Project (2012ZX07203-004). The authors gratefully acknowledge the fund from Shanghai Tongji Gao Tingyao Environmental Science and Technology Development Foundation.

References

1 A. Bhatnagar, W. Hogland, M. Marques and M. Sillanpää, *Chem. Eng. J.*, 2013, **219**, 499–511.
2 J. E. Kilduff, T. Karanfil and W. J. Weber, *Environ. Sci. Technol.*, 1996, **30**, 1344–1351.
3 G. Yang, L. Tang, Y. Cai, G. Zeng, P. Guo, G. Chen, Y. Zhou, J. Tang, J. Chen and W. Xiong, *RSC Adv.*, 2014, **4**, 58362–58371.
4 M. Molina-Sabio, M. T. Gonzalez, F. Rodriguez-Reinoso and A. Sepúlveda-Escribano, *Carbon*, 1996, **34**, 505–509.
5 M. Oschatz, L. Borchardt, I. Senkovska, N. Klein, M. Leistner and S. Kaskel, *Carbon*, 2013, **56**, 139–145.
6 Z. Huang, H. Shao, B. Huang, C. Li, Y. Huang and X. Chen, *RSC Adv.*, 2014, **4**, 18737–18743.
7 M. Myglovets, O. I. Poddubnaya, O. Sevastyanova, M. E. Lindström, B. Gawdzik, M. Sobiesiak, M. M. Tsyba, V. I. Sapsay, D. O. Klymchuk and A. M. Puziy, *Carbon*, 2014, **80**, 771–783.
8 P.-T. Yeung, P.-Y. Chung, H.-C. Tsang, J. Cheuk-On Tang, G. Yin-Ming Cheng, R. Gambari, C.-H. Chui and K.-H. Lam, *RSC Adv.*, 2014, **4**, 38839–38847.
9 L. Nielsen, M. J. Biggs, W. Skinner and T. J. Bandosz, *Carbon*, 2014, **80**, 419–432.
10 D. Ding, Y. Zhao, S. Yang, W. Shi, Z. Zhang, Z. Lei and Y. Yang, *Water Res.*, 2013, **47**, 2563–2571.
11 V. J. Watson, C. Nieto Delgado and B. E. Logan, *Environ. Sci. Technol.*, 2013, **47**, 6704–6710.
12 L. K. C. de Souza, N. P. Wickramaratne, A. S. Ello, M. J. F. Costa, C. E. F. da Costa and M. Jaroniec, *Carbon*, 2013, **65**, 334–340.
13 P. Chingombe, B. Saha and R. J. Wakeman, *Carbon*, 2005, **43**, 3132–3143.
14 B. Beckingham and U. Ghosh, *Environ. Sci. Technol.*, 2011, **45**, 10567–10574.
15 H. Liu, W. Liu, J. Zhang, C. Zhang, L. Ren and Y. Li, *J. Hazard. Mater.*, 2011, **185**, 1528–1535.
16 H. Liu, J. Zhang, N. Bao, C. Cheng, L. Ren and C. Zhang, *J. Hazard. Mater.*, 2012, **235–236**, 367–375.
17 S. Zuo, J. Liu, J. Yang and X. Cai, *Carbon*, 2009, **47**, 3578–3580.
18 D. Prahas, Y. Kartika, N. Indraswati and S. Ismadji, *Chem. Eng. J.*, 2008, **140**, 32–42.
19 A. J. Romero-Anaya, M. A. Lillo-Ródenas, C. Salinas-Martínez de Lecea and A. Linares-Solano, *Carbon*, 2012, **50**, 3158–3169.
20 A. M. Puziy, O. I. Poddubnaya, R. P. Socha, J. Gurgul and M. Wisniewski, *Carbon*, 2008, **46**, 2113–2123.
21 E.-A. Kim, A. L. Seyfferth, S. Fendorf and R. G. Luthy, *Water Res.*, 2011, **45**, 453–460.
22 M. I. Bautista-Toledo, J. Rivera-Utrilla, R. Ocampo-Pérez, F. Carrasco-Marín and M. Sánchez-Polo, *Carbon*, 2014, **73**, 338–350.
23 Y. Ono, Y. Amano, T. Nakamura and M. Machida, *Carbon*, 2012, **50**, 4984.
24 X. Tian, G. Hong, Y. Liu, B. Jiang and Y. Yang, *RSC Adv.*, 2014, **4**, 36316–36324.
25 B. Hong, X. Yu, L. Jiang, H. Xue, F. Liu, J. Li and Y. Liu, *RSC Adv.*, 2014, **4**, 33574–33577.
26 H. Liu, P. Dai, J. Zhang, C. Zhang, N. Bao, C. Cheng and L. Ren, *Chem. Eng. J.*, 2013, **228**, 425–434.

27 H. Liu, J. Zhang, C. Zhang, N. Bao and C. Cheng, *Carbon*, 2013, **60**, 289–291.
28 J. Wang, H. Liu, S. Yang, J. Zhang, C. Zhang and H. Wu, *Appl. Surf. Sci.*, 2014, **316**, 443–450.
29 Y. Kuno, M. Kojima, S. Ando and H. Nakagami, *J. Controlled Release*, 2005, **105**, 16–22.
30 J. J. M. Órfão, A. I. M. Silva, J. C. V. Pereira, S. A. Barata, I. M. Fonseca, P. C. C. Faria and M. F. R. Pereira, *J. Colloid Interface Sci.*, 2006, **296**, 480–489.
31 F. Suárez-García, A. Martínez-Alonso and J. M. D. Tascón, *Carbon*, 2004, **42**, 1419–1426.
32 M. A. Nahil and P. T. Williams, *Biomass Bioenergy*, 2012, **37**, 142–149.
33 H. Teng, T.-S. Yeh and L.-Y. Hsu, *Carbon*, 1998, **36**, 1387–1395.
34 Z.-L. Xie, R. J. White, J. Weber, A. Taubert and M. M. Titirici, *J. Mater. Chem.*, 2011, **21**, 7434–7442.
35 V. Fierro, V. Torné-Fernández and A. Celzard, *Microporous Mesoporous Mater.*, 2006, **92**, 243–250.
36 N. M. Haimour and S. Emeish, *Waste Manage.*, 2006, **26**, 651–660.
37 C. Srinivasakannan and M. Zailani Abu Bakar, *Biomass Bioenergy*, 2004, **27**, 89–96.
38 L. Wang, Y. Guo, B. Zou, C. Rong, X. Ma, Y. Qu, Y. Li and Z. Wang, *Bioresour. Technol.*, 2011, **102**, 1947–1950.
39 Y. Guo and D. A. Rockstraw, *Carbon*, 2006, **44**, 1464–1475.
40 V. Gómez-Serrano, E. M. Cuerda-Correa, M. C. Fernández-González, M. F. Alexandre-Franco and A. Macías-García, *Mater. Lett.*, 2005, **59**, 846–853.
41 V. Fierro, G. Muñiz, A. H. Basta, H. El-Saied and A. Celzard, *J. Hazard. Mater.*, 2010, **181**, 27–34.
42 Y. Guo and D. A. Rockstraw, *Microporous Mesoporous Mater.*, 2007, **100**, 12–19.
43 A. M. Puziy, O. I. Poddubnaya, A. Martínez-Alonso, F. Suárez-García and J. M. D. Tascón, *Carbon*, 2002, **40**, 1493–1505.
44 A. M. Puziy, O. I. Poddubnaya, A. Martínez-Alonso, F. Suárez-García and J. M. D. Tascón, *Carbon*, 2005, **43**, 2857–2868.
45 L. Huang, Y. Sun, T. Yang and L. Li, *Desalination*, 2011, **268**, 12–19.
46 D. Nabarlatz, J. de Celis, P. Bonelli and A. L. Cukierman, *J. Environ. Manage.*, 2012, **97**, 109–115.
47 M. C. Basso, E. G. Cerrella and A. L. Cukierman, *Ind. Eng. Chem. Res.*, 2002, **41**, 3580–3585.
48 F. Bouhamed, Z. Elouear, J. Bouzid and B. Ouddane, *Fresenius Environ. Bull.*, 2013, **22**, 3490–3500.
49 Q. Gao, H. Liu, C. Cheng, K. Li, J. Zhang, C. Zhang and Y. Li, *Powder Technol.*, 2013, **249**, 234–240.
50 H. Liu, X. Wang, G. Zhai, J. Zhang, C. Zhang, N. Bao and C. Cheng, *Chem. Eng. J.*, 2012, **209**, 155–162.
51 H. Liu, S. Liang, J. Gao, H. H. Ngo, W. Guo, Z. Guo, J. Wang and Y. Li, *Chem. Eng. J.*, 2014, **246**, 168–174.